Journal of *Marine Science and Engineering*

Article

Research on the Shock Environment Characteristics of a Marine Diesel Engine Based on a Large Floating Shock Platform

Yu Zhang [1,2,3], Jun Li [1,2], Chunhui Zhang [3], Wei Chen [1,2], Zhipeng Du [3] and Xiaobin Li [1,2,*]

1 Key Laboratory of High-Performance Ship Technology, Ministry of Education, Wuhan University of Technology, Wuhan 430063, China; 319054@whut.edu.cn (Y.Z.); ljy60023@sina.com (J.L.); whutcw01@126.com (W.C.)
2 School of Naval Architecture, Ocean and Energy Power Engineering, Wuhan University of Technology, Wuhan 430063, China
3 Naval Research Academy, Beijing 100161, China; 15042694716@163.com (C.Z.); duzp7755@163.com (Z.D.)
* Correspondence: lxbmark@163.com

Abstract: To conduct a precise shock assessment of marine diesel engines, a 200 t floating shock platform was utilized to simulate realistic testing conditions. The testing generated the acceleration time curve and the shock response spectrum for the diesel engine. According to the applicable standards, the spectral velocity was chosen as the evaluation index, and an evaluation of the longitudinal, transverse, and vertical shock environment of the diesel engine was conducted. The shock factor interpolation method was corrected using the confidence interval based on normal distribution, and the interpolated confidence interval of the shock factor was determined. The findings reveal that shock waves were identified as the primary external force, and it was found that the influence of bubble pulsation can be disregarded when assessing a floating shock platform. This paper proposes the use of normal-distribution-based shock factor confidence intervals, which can accurately predict multidirectional shock factors and offer improved shock safety compared to the traditional method of unidirectional shock factor interpolation. The results and methods obtained in this study can provide valuable guidance and assistance for predicting the shock environment of large shipboard machinery on significant floating shock platforms.

Keywords: large-scale floating shock platform (LFSP); shock environments; underwater explosion; marine diesel engines; shock spectra

Citation: Zhang, Y.; Li, J.; Zhang, C.; Chen, W.; Du, Z.; Li, X. Research on the Shock Environment Characteristics of a Marine Diesel Engine Based on a Large Floating Shock Platform. *J. Mar. Sci. Eng.* **2023**, *11*, 2308. https://doi.org/10.3390/jmse11122308

Academic Editor: Carlos Guedes Soares

Received: 25 October 2023
Revised: 28 November 2023
Accepted: 4 December 2023
Published: 6 December 2023

1. Introduction

Shipboard equipment shock resistance is a crucial aspect of a ship's combat effectiveness and survivability [1]. To ensure the ship's survival rate in modern naval warfare, navies have developed numerous shock testing devices to assess the shock resistance of shipboard equipment and have established relevant assessment standards [2,3]. The US standard MID-901D [4] mandates that shipboard equipment weighing less than 181 t must undergo shock testing before being put into service. In order to evaluate medium and large shipboard equipment, the United States constructed a multi-level floating platform to assess various levels of equipment.

China began in the field of shock resistance later, and mainly developed its floating shock platform from research on the American platform. Chen [5] employed the wavelet transform approach to analyze measurement signals from a small-scale floating platform (SFSP), and observed that the predominant shock response of the SFSP is high-frequency vibration following shock waves' shock. Jiang [6] employed shock wave loads directly applied to the blast-facing surface of the computational flow field to simulate the shock response of the floating platform under far-field explosion conditions. This approach compensates for the finite element software's limitations in far-field calculations. Chen [7] developed a small floating platform using the acoustic solid coupling approach of finite element analysis, and verified the effectiveness of the simulation method through actual explosion results. Scholars have conducted experimental and simulation studies on small floating platforms to provide a dependable foundation for medium- and large-scale equipment. Chen's [8] development of a standard floating platform shock environment test in China was analyzed and compared with the equivalent standard in the US. The results indicate that the shock spectra of both standards are essentially identical. Wang [9,10] analyzed and verified the discrepancy between the shock environment of a medium-sized floating platform based in the UK and a real ship using Fisher's method. Furthermore, they investigated the effect of each parameter of the shock spectrum on the multi-degree-of-freedom system through theory and simulation. Jin [11] systematically designed a medium-sized floating platform and analyzed various typical floating platform structures using finite element analysis. The results indicate that the structural strength of the low bulkhead-box beam structure meets the German standard in terms of its shock environment. Zhang [12] conducted a preliminary investigation into the shock response of the standard floating platform and large floating platform in the installation of equipment when subjected to different blast distances under fluid–structure coupling. The scholars mentioned above conducted research on the U.S. floating platform, which provides a useful reference for China's development of its own floating shock platform. This will aid in the promotion of China's newly developed large-scale shipboard equipment in the field of shock assessment.

In recent years, China has constructed floating shock platforms in various tonnages, ranging from 8 t to 200 t. A small-scale floating shock platform has a maximum bearing capacity of 8 t, while a standard floating shock platform can carry between 2.7 t and 50 t. Additionally, the floating shock platform offers a 100-tonne capacity and can effectively perform shock assessment tests on ship equipment, the equipment base, and elastic components, making it an essential experimental platform for simulating the shock resistance of actual ships. These platforms allow for the testing of newly developed large shipboard equipment, including diesel engines and gas turbines. For a 200-tonne-class floating shock platform, Yang [13] investigated the shock of spherical factors on simulated shock environments, and analyzed the low-frequency response of the platform. Zhang [14] analyzed the low-frequency oscillator data of a 200-tonne floating shock platform used for underwater explosion testing. The results indicate that the floating platform's low-frequency response is mainly dominated by the overall rigid body motion, and the difference in low-frequency shock response between its components is not significant. Feng [15] designed a broader cross-drop ratio of the inclined baffle structure through simulations and calibration tests. Insufficient experimental data are available for the 200-tonne-class floating shock platform, which hinders researchers from conducting a thorough study of its shock environment. Zhang [16] analyzed the variation of the shock environment of the explosion-facing surface, the back-explosion surface and the mid-longitudinal profile, and found that the shock spectrum of the back-explosion surface had a sharp peak, resulting in the spectral velocity of the back-explosion surface being greater than that of the explosion-facing surface, and the displacement value of the back-explosion surface being greater than that of the explosion-facing surface. The shock environment serves as input to resist shock and is crucial for finite element analysis. To address this, the shock factor interpolation method has emerged as a reliable approach. This method fits parameters based on test data, shock factor, and shock response spectrum, which effectively provides shock input for finite element analysis of related equipment, resulting in significant cost savings. Previous research [17–20] only considers the one-way effect of the transverse longitudinal pendant in shock environmental forecasting methodology, and only takes into account its one-way error. However, in actual experiments, the explosion data are discrete, and should be allowed to have a certain margin of error. This paper suggests using a normal distribution based on the shock environment forecasting method to analyze the data. The method includes the discrete and multi-directional shock factors and utilizes interpolation fitting. It provides a placeability interval that has a higher shock safety, obtained through the interpolation interval formula.

In this paper, we conduct an assessment of the shock environment characteristics of a large-scale floating shock platform on a marine diesel engine. Specifically, we utilize a shock assessment test carried out on a 200-tonne floating platform to analyze the shock on the engine. During the experiment, we developed two longitudinal assessment conditions and four transverse assessment conditions. We collected acceleration data in the transverse, longitudinal, and vertical directions, and processed them to obtain the shock response spectrum at each measurement point. We analyzed and assessed the typical shock spectrum of each working condition at the same measurement point based on HJB715-2016 [21]. It was discovered that the evaluation criteria regarding the shock environment meet 70% of the standard shock spectrum criteria. Furthermore, the spectral velocity garnered from the assessment shows a linear correlation with the shock factor; however, the degree of dispersion is excessive. This suggests that current standards only adhere to shock assessment test evaluation standards. Therefore, previous studies have limited their data selection in a singular horizontal and vertical direction to conform to the shock factor interpolation. In this paper, we propose a confidence interval based on the normal distribution to interpolate and fit data along the horizontal, vertical, and depth directions. The experimental data are distributed within their respective ranges, indicating that our interval estimation method is more suitable for the discreteness of explosion data, and can better predict the shock environment. Technical term abbreviations will be explained upon first use, and consistent citation and footnote styles will be adhered to.

This paper focuses on marine diesel engine testing and presents its structure in Section 2. The chapter also introduces the accelerometer parameters of the test object, the large-scale floating shock platform used in the test, and the assessment test design. Additionally, it discusses the shell shock factor. Section 3 talks about the test data evaluation index basis and data analysis methodology. It proposes a permissible interval prediction method based on the normal distribution. Section 4 details the experimental results and discusses acceleration, shock response spectrum, and the interpolation formula for the confidence interval. It proposes the advantages of using the confidence interval over previous studies. The primary conclusion of this paper is in Section 5.

2. Experimental

2.1. Subject

Middle and high-speed diesel engines, along with related equipment such as accessory pumps, sliding oil filters and coolers, and electric control boxes, are displayed in Figure 1. The medium- and high-speed diesel engines are installed together with a test generator and two other types of equipment in the center of the testing platform. The auxiliary generator is installed at the end of the platform, and two measurement buffer platforms are installed at the beginning. The B&K4384 acceleration sensor is shown in Figure 2, and the parameters are shown in Table 1.

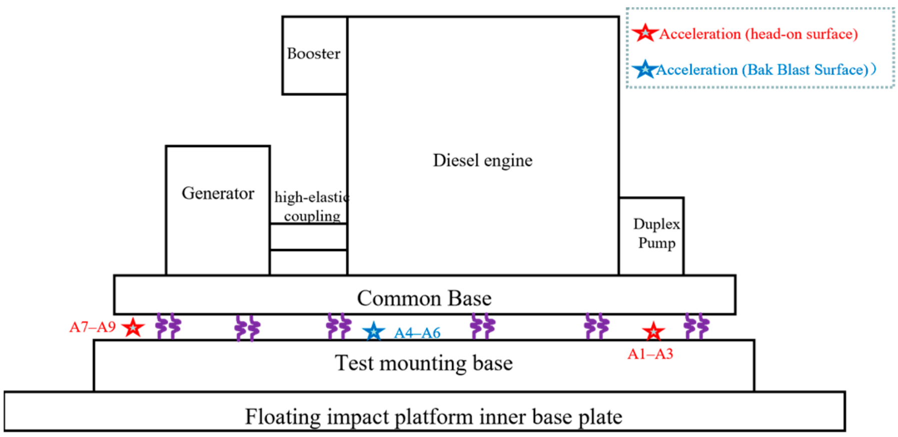

Figure 1. Diesel engine and measurement point arrangement.

Figure 2. Acceleration sensors.

Table 1. B&K4384 Sensor parameters.

B&K4384	Charge Sensitivity (pc/g)	Voltage Sensitivity (mv/g)	Mounted Resonance (KHz)	Frequency Range (Hz)
Parameters	9.8 ± 2%	8 ± 2%	42	0.2~9100

2.2. Design

The test platform for 200 t level floating shock platform. The platform has a total length of 19 m, a total width of 9.1 m, and a total height of 7 m. The internal effective height is 6 m, the double bottom height is 1 m, and the ramp height is 0.5 m. The maximum draft is 3 m, and it can accommodate up to 200 t of test equipment.

A diesel engine and associated equipment were utilized to conduct six underwater explosion shock tests in two positive directions: longitudinal and transverse. The experiment utilized an explosive source of 150 kg TNT, and the design is depicted in Figure 3. The TNT standard explosive source is positioned on the side of the pontoon either transversely (along the width of the ship) or longitudinally (along the length of the ship) for detonation, the explosion test diagram is shown in Figure 4.

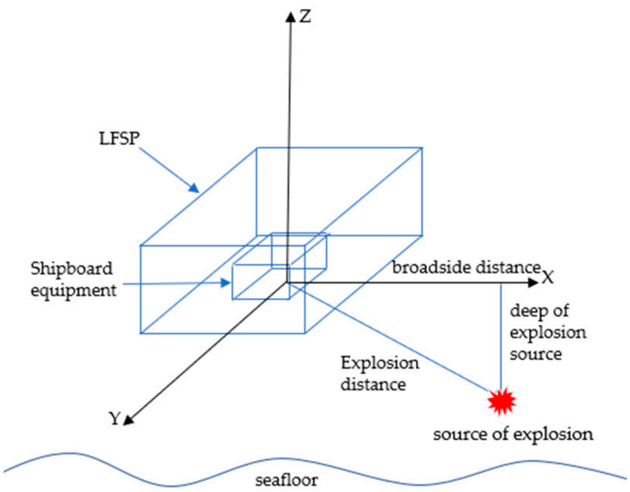

Figure 3. Schematic diagram of the experiment.

Experiment: The shock of the experiment is divided into two groups, A and B, with a total of 18 channels designated for measurement points to determine the environmental shock. The measurements are labeled X for lateral, Y for longitudinal, and Z for vertical.

2.3. Shock Factor

The shock environment's strength resulting from an underwater explosion is commonly determined by the shock factor. As defined in Equation (3), this factor is calculated using the shell plate shock factor (*HSF*) [22].

$$HSF = \frac{\sqrt{W}}{R} \tag{1}$$

where *HSF* is the shell plate shock factor; *W* represents the charge equivalent taking into account the seabed reflection coefficient, whose unit is kg; and *R* denotes the minimum distance between the explosion source, whose unit is m.

Figure 4. Underwater explosion experiment.

During the experiment, external factors like currents, wind, and waves on the port side, as well as the depth of the explosion source cloth, may affect the size of the shock factor. To reduce these effects, we used a positioning system to determine the platform and relative position of the explosion source. Table 2 shows the experimental explosion distance and shell plate shock factor. Upon analyzing the test data, we found that the shock factor increases when the burst distance is closer, indicating that greater shock energy leads to a more intense degree of explosion. Additionally, the burst distance and the shock factor are inversely proportional.

Table 2. Test burst distance and impact factor.

Test	Direction of Test	Explosion Distance (m)	Shock Factor
1	Longitudinal	10.319	1.46
2		12.694	1.20
3	Horizontal	13.901	0.997
4		15.552	0.862
5		16.520	0.828
6		17.789	0.756

3. Experimental Analysis Methods

3.1. Data Assessment Basis

When installing marine diesel engines for Class A equipment, it is important to ensure the location is suitable for Class I and that the equipment allows for flexible installation. According to GJB1060.1-91 [23], if the equipment mass exceeds 5 t, the isolation system, shock spectral velocity, and acceleration should be discounted. After assessing the shock on the environment, the discounted impact assessment spectrum can be derived using Formulas (2) and (3), and the assessment spectrum is shown in Table 3.

$$\frac{A}{A_0} = (\frac{m}{m_0})^{(-0.537)} \tag{2}$$

$$\frac{V}{V_0} = (\frac{m}{m_0})^{(-0.4)} \tag{3}$$

where m is the mass of the equipment installed in isolation, m_0 is the mass constant, and the constant equal to 5 t. A is the discounted acceleration spectral value, and A_0 is the same acceleration spectral value, whose unit is g. V is the discounted velocity spectral value, and V_0 is the same velocity spectral value, whose unit is m/s.

Table 3. Shock environment assessment requirements.

Installation Part	Orientations	Iso-Acceleration Spectrum a_0 (g)	Iso-Velocity Spectrum v_0 (m/s)	Iso-Displacement Spectrum D_0 (cm)
Class I	Vertical	320	7.0	4.3
	Horizontal	280	6.0	3.0
Discounted class I	Vertical	63.71	2.10	4.3
	Horizontal	55.74	1.80	3.0

3.2. Acceleration Data Analysis Method

As stated in HJB715-2016, the original acceleration data are analyzed using the least-squares method to eliminate its trend term. The Butterworth filtering function is used to filter the frequency range between 4–400 Hz, which greatly affects the equipment's response. According to ISO18431 [24], the measured acceleration data are transformed into the shock spectrum from the shock environment. By obtaining data from the isotropic displacement value of the low-frequency array and the low-frequency segment curve of the shock spectrum, the low-frequency interference is eliminated through frequency filtering. The shock spectrum's frequency is then high-pass-filtered to obtain the measured spectrum. The captured spectrum is calibrated to derive the calibrated spectrum, which represents the shock environment at the measurement point. When compared to the calibrated spectrum, the captured spectrum meets the required specifications:

1. The spectrum being measured is at least 70% similar to the standard spectrum;
2. There must be at least two points where the measured spectrum intersects the normalized spectrum within one octave of the frequency range below the normalized spectrum;
3. The area under the measured spectrum should not exceed the area under the standard spectrum.

3.3. A Shock Environment Prediction Method Based on Normal Distribution

This paper presents an interpolation formula that determines the correlation between three-way spectral velocity and the shell-plate shock factor using experimental data. In addition, confidence intervals for the lognormal distribution are obtained. The *S-N* (stress-life) curve approach commonly uses the lognormal distribution in fatigue testing, and this method transforms the original non-linear power function formula into a linear representation [25]. The assumption behind this method is that the specimens' structure and testing conditions remain constant throughout the tests. 1. Multiple and distinct data points are collected. 2. The data are distributed over several levels, with each level containing at least three data points of the same magnitude.

When attempting to predict shock environments, several measuring points and challenges arise when collecting data and accounting for the volatility of explosion tests. To account for errors in the statistics of the measuring points, confidence intervals are required. Equations (4) and (5) provide the necessary corrections.

To achieve a 50 percent survival rate, use the following formula:

$$V = aC + b \tag{4}$$

To achieve a 97.7 percent survival rate, use the following formula:

$$V = aC + b - 2\sigma \tag{5}$$

where V is the spectral velocity, C is the shock factor, a is the slope, b is the intercept, and σ is the standard deviation.

The simulation data and forecasting method presented in Equation (6) from the literature [13] were compared to normal-distribution-based interpolated confidence intervals for validation.

$$\begin{cases} \varepsilon = \left|\frac{x_A - x_F}{x_F}\right| \times 100\% \\ \varepsilon_{\max} = \max\{\varepsilon_i\}, i = 1, 2, 3 \cdots \end{cases} \tag{6}$$

where is the actual value, is the forecast value, is the relative error of the forecast, and is the maximum relative error.

4. Experimental Result and Discussion

During offshore explosion shock testing, we arranged 18 channels in the medium- and high-speed diesel engine mounting base panel. These channels were divided into two groups, A and B, to measure the shock environment. We numbered the measurement points A1–A9 and placed six channels on the blast face and three channels on the back of the blast face to measure the longitudinal, transverse, and vertical shock acceleration responses of the motor base. We recorded a total of 108 measurement points, with a validity of 76.8%. However, only 27.5% were valid under working Condition 6. The measured point data after comparison are shown in Table 4. Next, the data from various circumstances at standard measuring points are chosen for comparative examination.

Table 4. Test conditions and measured regularization spectrum values.

Measuring Points	Direction of Test		Spectral Velocity (m/s) Test 1	Test 2	Test 3	Test 4	Test 5	Test 6
A1	The face of the blast surface	Horizontal	1.81	1.66	2.13	1.58	1.61	6.13
A2		Longitudinal	1.56	2.09	2.39	1.49	1.57	2.64
A3		Vertical	2.3	2.42	2.19	2.80	1.89	1.81
A4	Backblast surface	Horizontal	1.37	1.19	2.19	2.14	2.00	2.64
A5		Longitudinal	1.63	1.44	1.14	1.17	0.55	1.52
A6		Vertical	1.75	2.02	3.49	3.18	3.04	253.01
A7	The face of the blast surface	Horizontal	1.36	1.21	3.1	2.04	1.7	2826.2
A8		Longitudinal	1.7	1.48	1.35	1.03	0.92	20.41
A9		Vertical	1.85	1.58	3.94	3.18	2.58	33.45

4.1. Acceleration Time-Course Curve Analysis

In Figure 5, it is shown that the acceleration peaks of longitudinal evaluation Test 1 and Test 2 are similar. The primary factor is that the disparity in distance between Test 1 and Test 2, and the explosion's origin is approximately 2 m. The shock wave did not weaken within this 2-m distance. Combined with the peak value of 981.2 g in Test 3 of Figure 6, this indicates that the shock wave remains in a stable range between 0 and 14 m and does not decay.

In Test 1, the main peak reaches 773.27 g at 0.114 ms, and a second peak of 132.01 g occurs at 1.01 ms. For Case 2, the peak acceleration reaches 786.18 g at 0.221 ms, and a second peak of 254.07 g appears at 1.08 ms.

Figure 6 illustrates the results of the transverse plumbing examination of Test 3, which revealed two peaks: 982.28 g at 0.055 ms for the first peak, and 76.79 g at 0.894 ms for the second. For Tests 4–6, the respective peaks were 888.48 g, 637.18 g, and 523.03 g at 0.114 ms, 0.107 ms, and 0.110 ms, as shown in Figure 6. However, the second peak for Tests 4–6 was not observed.

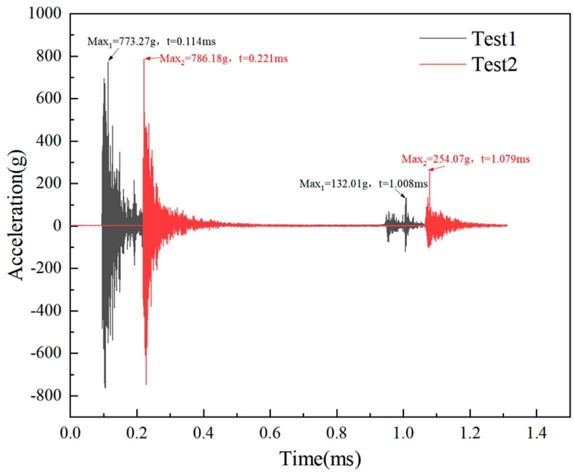

Figure 5. Acceleration–time curve of the longitudinal test condition.

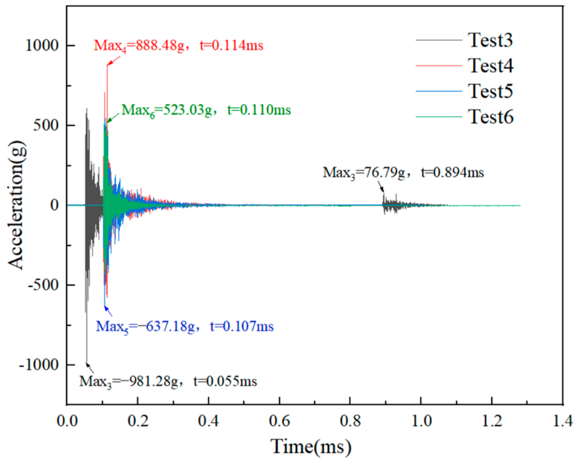

Figure 6. Acceleration–time curve of the horizontal test condition.

When comparing Figures 5 and 6, it is clear that the peak acceleration decreases as the shock factor decreases, demonstrating a linear relationship. Additionally, the longitudinal test condition has a greater shock factor, but the peak acceleration in Conditions 1 and 2 is lower than that in Conditions 3 and 4. This could be due to the influence of different structures during the transmission of the shock wave in both transverse and longitudinal directions. These structures can weaken the effect. From the measured data, it is apparent that the shock caused by bubble pulsation is significantly smaller than the shock wave for the floating shock platform equipment. This equipment is the primary source of external force. Therefore, the effect of bubble pulsation can be disregarded during shock assessments of said equipment.

4.2. Shock Environment Analysis and Assessment

The diesel engine with a limiter has a vertical installation frequency of 14.6 Hz, a horizontal frequency of 22.9 Hz, and a longitudinal frequency of 15.8 Hz. During the explosion shock loading stage, the vibration isolator shows shock stiffness characteristics, which cause the installation frequency of the medium- and high-speed diesel engine system to increase to around 20 Hz. Based on the analysis, the frequency range that mainly affects the shock response of the medium and high-speed diesel engine is 10 Hz to 100 Hz. The environment's shock characteristics in this frequency range are primarily measured using spectral velocity. Therefore, the strength of the test data's shock is evaluated using spectral velocity as the assessment index. We processed the measured data to obtain the typical shock response spectral curve of A3, which is illustrated in Figures 7 and 8, and the regularized spectral values in Table 3.

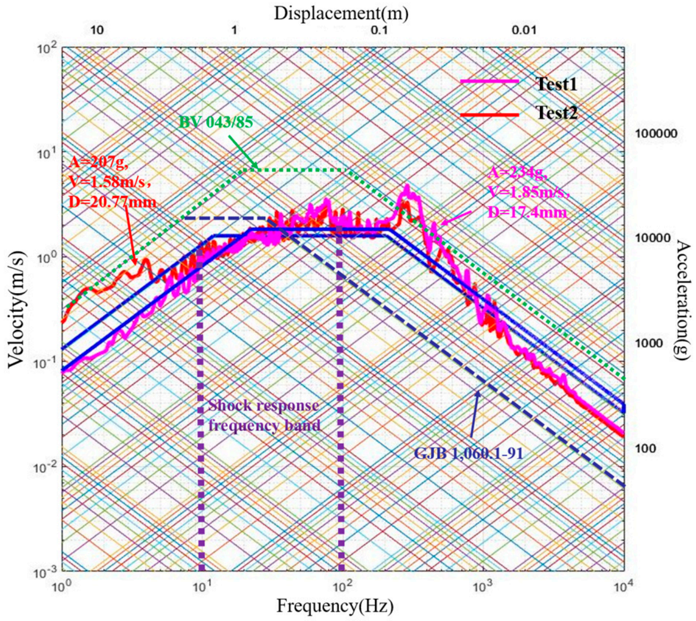

Figure 7. Typical shock spectrum for longitudinal examination.

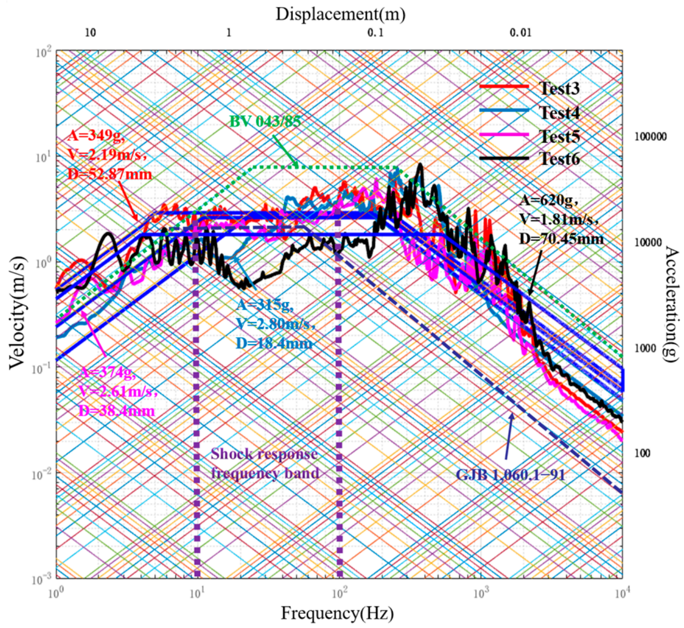

Figure 8. Typical shock spectrum for horizontal examination.

Figures 7 and 8 show that the German military standard BV 043/085 [2] takes into account the quality of equipment and its shock on the environment when assessing the vertical spectral velocity. The BV 043/085 requires the velocity to be at 7.0 m/s. On the other hand, the GJB1060.1-91 reduces the vertical assessment of spectral velocity to 2.1 m/s for equipment weighing more than 5 t, as specified in Section 2.1. Figures 8 and 9 depict six working conditions for longitudinal, horizontal, and vertical assessment, which have met over 70% of the assessment criteria in terms of spectral velocity.

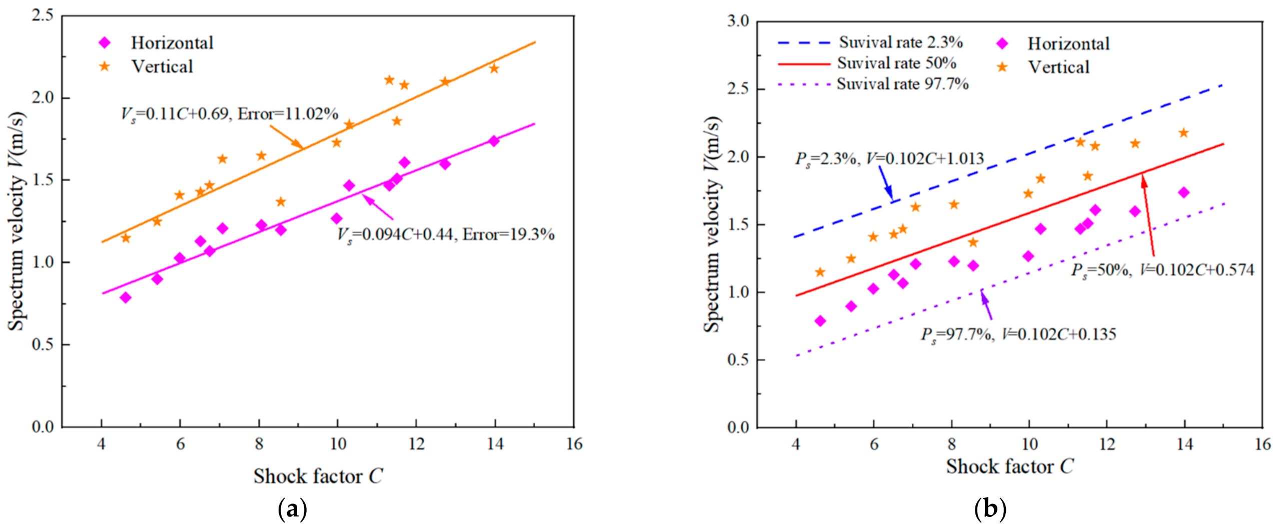

Figure 9. Comparison of methods for forecasting shock environments: (**a**) error interpolation formula; (**b**) confidence interval forecast.

In Figures 7 and 8, we can see that Test 1 has a spectral velocity of 1.85 m/s, which is higher than Test 2's velocity of 1.58 m/s. When looking at the longitudinal test cases, only Test 1's spectral velocity exceeds that of transverse Test 6 (1.81 m/s), while Test 2 falls behind the other cases. As we saw in Section 3.1's acceleration–time curve, the shock strength of the longitudinal test conditions is generally lower than that of the transverse test conditions. This is because the shock wave attenuates twice as much along the ship's length than its width.

Figure 7 shows the longitudinal assessment of conditions in the low-frequency stage below 20 Hz and below 10 Hz. Test 2 has significantly higher spectral displacement than Test 1, while frequencies of 10 Hz to 20 Hz show consistency between the two. In the high-frequency stage, both conditions are basically the same. For the main frequency range between 10 Hz and 100 Hz, the spectral velocity of Test 1 is slightly higher than that of Test 2. This result is in line with the law that indicates the bigger the shock factor, the higher the shock intensity.

In Figure 8, it is evident that spectral displacement significantly differs in transverse vertical assessment conditions below 20 Hz. All high-frequency bands, with the exception of Test 6, exhibit consistency. The test data reveal that the efficiency of Condition 6 is only 5%, which is speculated to be caused by sensor malfunction due to reduced filtering function after several explosion tests. The frequency range of 10 Hz to 100 Hz has the most significant effect, while the remaining conditions experience a decreasing spectral velocity in consecutive order. Although Test 3 has a lower shock than Tests 4 and 5, it still meets the assessment requirements. Combining the test data, it can be concluded that individual conditions do not meet the assessment requirements when the shock factor is higher. The law indicates that the higher the shock strength, the greater the shock factor. However, overall, the assessment requirements are still being followed.

4.3. Shock Environment Prediction

According to Figure 9a in the literature [13], the maximum error in the transverse direction is 19.3%, with a slope of 0.094. Similarly, the maximum error in the vertical direction is 11.02%, with a slope of 0.11. The prediction equations depend on the slope and shock factor, which determine the strength of the shock intensity. The fit of the method is not significantly different in the transverse direction (0.094) and the vertical direction (0.11), suggesting that the shock intensity suffered in these two directions is similar. Therefore, there is not much variation between the transverse direction and the vertical direction for the same shock factor.

In Figure 9b, the simulated data are shown to fall within the confidence intervals. The vertical data are mostly distributed between survival rates of 50% and 2.3%, while the lateral data fall completely within the 50% and 97.7% intervals. Confidence intervals provide a more understandable representation of the distribution of lateral and vertical data compared to past methods. Using these data, the fitted shock environment can predict multidirectional shock environments.

Based on Figures 10 and 11, it appears that there is a direct relationship between the shock factor and the spectral velocity. However, Figure 10b reveals that the actual data appear to be discontinuous. This can be seen in the longitudinal spectral velocity from Figure 10a and the transversal spectral velocity from Figure 11. Figure 11a shows a decrease in trend as the shock factor increases, while in Figure 10a, the transverse spectral velocity is generally higher than the longitudinal spectral velocity, which differs from previous research. These differences could be due to the lack of experimental data in previous studies or the ideal simulation conditions. Additionally, the shock of complex sea states was not considered.

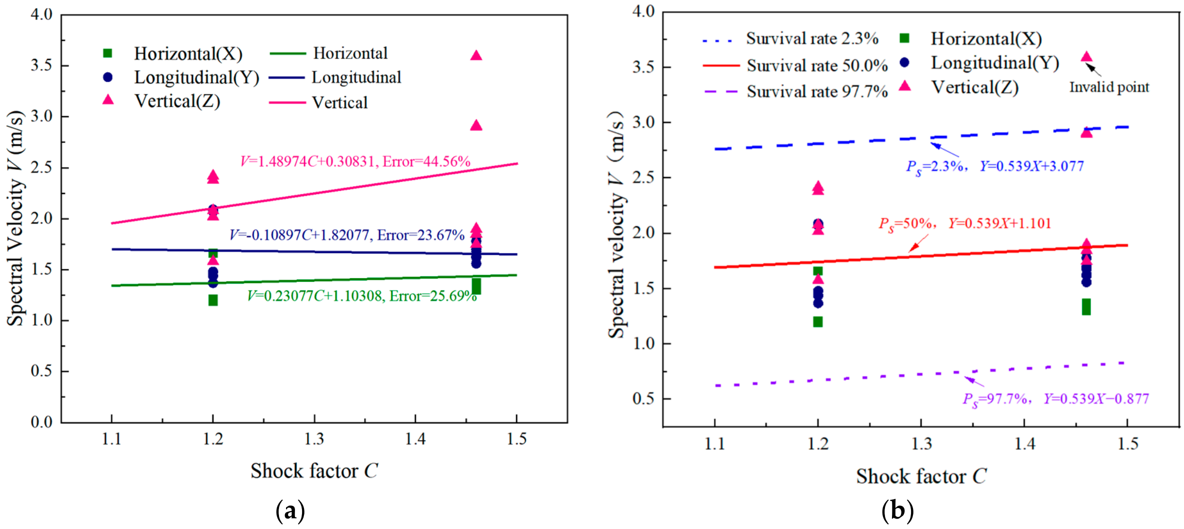

Figure 10. Longitudinal condition shock environment prediction: (**a**) error interpolation formula; (**b**) confidence interval forecast.

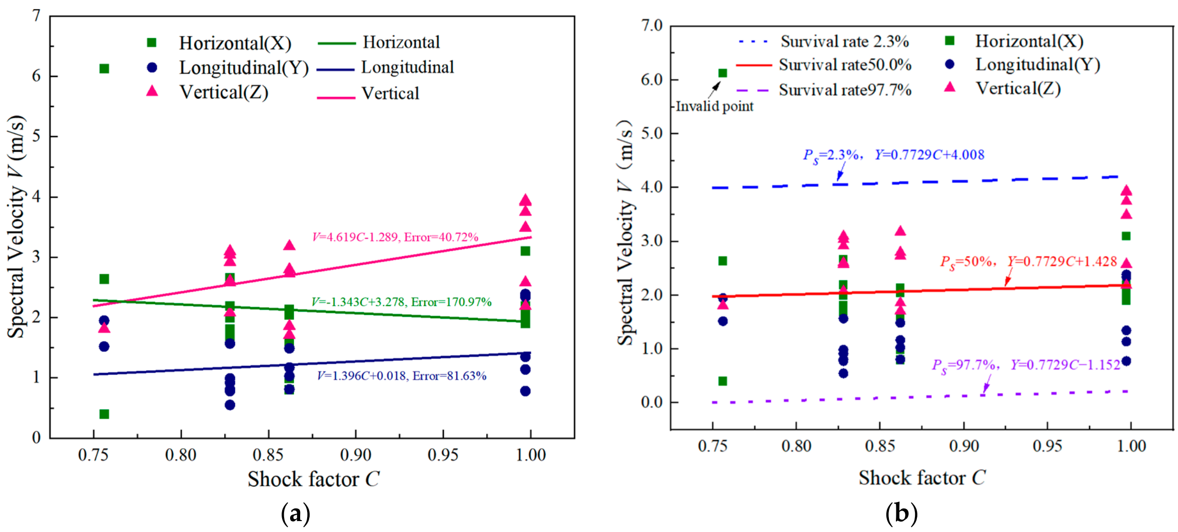

Figure 11. Horizontal condition shock environment prediction: (**a**) error interpolation formula; (**b**) confidence interval forecast.

Based on Figures 10b and 11b, there is a clear positive correlation between the shock factor and the three-way spectral velocity. The vertical spectral velocities consistently fall within the upper 50% survival rate interval, while the horizontal and longitudinal spectral velocities fall within the lower interval. It is important to note that some individual data points fall outside the confidence interval. This indicates that the confidence interval helps to eliminate invalid data and improve the accuracy of the interpolation formula. By integrating the spectral velocity values obtained, the shock intensity can be substituted. This approach is useful for analyzing isolated experimental data and predicting three-way spectral velocity and shock factor.

When predicting the shock of an explosion on the environment, various factors come into play, such as the state of the sea, angle of attack, explosive charge, and distance of the explosion. However, in simulation conditions, the state of the sea is pre-calculated and does not affect the other conditions. The data received from the shock environment are then filtered through a large-scale floating shock platform, resulting in accurate data that typically have a greater vertical dimension than horizontal, and a greater horizontal dimension than longitudinal.

Figure 9 shows that the forecast formulas for unidirectional data and shock factors using confidence intervals are just as precise as the error analysis approach in simulation circumstances. However, when predicting multidirectional shock environments, confidence intervals are more advantageous.

During the field tests, the shock of the sea state on the blast distance and angle of attack was not consistent, resulting in highly discrete data. In order to effectively handle this, the prediction method based on interval estimation was utilized. When predicting multidirectional shock environments, the multidirectional spectral velocities are uniformly distributed in intervals, which visually demonstrates the characteristics in the specification. For instance, the lateral spectral velocities are 50 to 85 percent of the vertical spectral velocities, and the longitudinal spectral velocities are 25 to 33 percent of the vertical velocities.

Through the acceleration time history curve of the measurement point, as shown in Figures 5 and 6, this study observed the bubble pulsation phenomenon. It was found that the phenomenon occurred mainly when the shock factor was large. However, the acceleration peak caused by it was much smaller than the peak caused by the shock wave. Thus, the influence of bubble pulsation can be ignored. Furthermore, by analyzing the typical shock spectrum of Figures 7 and 8, the study found that the main inflection point of the positive and horizontal evaluation conditions occurred between 4 and 20 Hz. The main inflection point of the positive and longitudinal evaluation conditions was between 10 and 20 Hz. The spectral displacement value of the working conditions between 4 and 10 Hz was much larger than that of the 10–20 Hz working conditions, which is in accordance with the literature [15]. The study also found that the bubble pulsation phenomenon was observed in working conditions 1 and 2 at 10–20 Hz. Meanwhile, the bubble pulsation phenomenon was observed only in working condition 3 with the largest shock factor at 4–20 Hz. This finding is consistent with Ref. [15] and Figures 5 and 6. It indicates that the low-frequency rigid body motion of the floating platform caused by bubble pulsation is more obvious when the shock factor is larger. The shock strength is weakened to a certain extent, which does not lead to the low-frequency rigid body motion of the floating platform.

Based on Table 3 and Figures 7 and 8, we can see that the average spectral velocity of the blast surface is slightly higher than that of the back-burst surface under positive and longitudinal assessment conditions, which contradicts the previous finding from Ref. [16], which suggested the opposite result. Although the difference is small, it may be due to unforeseen circumstances during the experiment. Nevertheless, the forecast formula for a devastating environment in reference material is still reliable [16]. The data have been interpolated and fitted in one direction, leading us to conclude that the vertical shock environment is more severe than the lateral and longitudinal ones. As shown in Figures 10 and 11, the survival rate of 2.3–50% is where vertical data are mainly distributed, while horizontal data are centered around the 50% survival rate, and longitudinal data fall between 50% and 97.7%. Since the assessment standard only requires the test data to reach 70% of the assessment standard without specifying an upper limit, this implies that shipboard equipment can pass the assessment simply by improving its quality, regardless of the equipment's economic feasibility. By using confidence interval interpolation fitting, we can set the upper and lower limits of data that meet the assessment standard, which helps us regulate the economic costs of shipboard equipment.

Furthermore, the confidence interval helps to determine the shock intensity level (*HSF*) and the blast source's shock intensity (a). Adjustments to constant b occur after considering the blast source's distance and the shock of the relevant structure during transmission. This approach offers a new avenue for future research. However, the integration of the shock wave attenuation formula into the shock environment prediction formula is beyond the scope of this study. Targeted experiments will be required for this purpose at a later stage.

5. Conclusions

To guarantee that the 200-tonne-class floating shock platform offers the required shock assessment data for the marine diesel engine, six underwater explosion experiments were conducted to assess the shock environment. The characteristics of the shock environment on the marine diesel engine under the large-scale floating shock platform were studied, and the forecasting method for the shock environment was improved. This will provide a reference for the shock environment of large-scale shipborne equipment in a large-scale floating shock platform for shock resistance testing. The key findings are as follows:

(1) The primary external force acting on the marine diesel engine of the floating shock platform is the shock wave. Low-frequency rigid-body motion is caused by bubble pulsation only when the $HSF \geq 1$. When the $HSF < 1$, bubble pulsation has a negligible shock.
(2) In the positive longitudinal assessment conditions, the shock factor is greater than in the positive transverse assessment conditions. However, the peak acceleration is slightly smaller in the former than in the latter. This can be attributed to the aspect ratio of 2:1 of the floating shock platform. The experimental design only took into consideration the distance from the source of the burst on the outboard side, but not the length and width ratio of the floating shock platform. Hence, future test designs should consider this aspect to improve accuracy.
(3) The spectral velocity of the floating shock platform on the ship's diesel engine facing the explosion surface is slightly greater than that of the back explosion surface. However, this difference is not significant, contradicting the previous findings of finite element analysis. Nevertheless, there continues to be a linear relationship between the spectral velocity and shock factor, with an increase in spectral velocity corresponding to an increase in shock factor.
(4) This paper presents a normal distribution that relies on the confidence interval for shock environment forecasting while considering discrete test data. The method provides an accurate forecast for the three-way shock environment in the horizontal and vertical directions. Compared with previous research using unidirectional methods, equipment shock safety can be assessed at a higher level.

Author Contributions: Investigation, Validation, Writing—original draft preparation, Y.Z.; Writing—review and editing J.L.; Resources, Data curation, C.Z.; Supervision, Writing—review and editing, W.C.; Supervision, Data curation, Writing—review and editing Z.D.; Funding acquisition, Writing—review and editing, X.L. All authors have read and agreed to the published version of the manuscript.

Funding: This research was funded by the National Natural Science Foundation of China (51979213).

Institutional Review Board Statement: In this section, you should add the Institutional Review Board Statement and approval number, if relevant to your study.

Informed Consent Statement: Not applicable.

Data Availability Statement: The authors declare that the data presented in this study are available on request.

Acknowledgments: This paper is supported by the National Natural Science Foundation of China (51979213).

Conflicts of Interest: The authors declare no conflict of interest.

References

1. Wang, Y.; Hua, H.X. *Modern Shock Theory and Application of Ships*; Science Press: Beijing, China, 2006.
2. *BV0430/85*; Code for Ship Construction-Shock Safety. FRG Ministry of Defense Equipment Technology and Procurement: Koblenz, Germany, 1985.
3. *GJB150.18-1986*; STIC Military Standards Center. Environmental Test Methods for Military Equipment-Shock Test. Standards Press of China: Beijing, China, 1986.
4. *MIL-S-901D*; Military Specification: Shock Tests. H.I. (High-Shock) Shipboard Machinery, Equipment, and Systems, Requirements. U.S. NAVY: New York, NY, USA, 1989; pp. 70–72.
5. Chen, J.J.; Zhang, S.H.; Mao, Q.D. Analysis of shock response of small-sized floating platform in underwater explosion. *Noise Vib. Control* **2012**, *32*, 30–33.
6. Jiang, G.; Jin, H.; Wang, Y.; Zhou, X. Study on shock response of floating platform subjected to far-field explosion. *Acta Armamentarii* **2010**, *31*, 37–40.
7. Chen, G.J.; Zhou, Q.F.; Wang, S.L. Numerical simulation test and validation of a small floating shock platform subjected to undex. *Electron. Meas. Technol.* **2016**, *39*, 42–44, 52.
8. Chen, X.B.; He, B.; Chen, H. Test and analysis about the shock environment of standard floating shock platform. *Acta Armamentarii* **2014**, *35*, 8–12.
9. Wang, J.; Guo, J.; Yao, X.L. Discriminant analysis on the shock environment of floating shock platform as opposed to real ship. *J. Vib. Shock* **2014**, *33*, 108–112. (In Chinese)
10. Wang, J.; Yao, X.L.; Yang, D. Shock analysis of shock environment from floating shock platform equipment response. *Explos. Shock Waves* **2015**, *35*, 236–242.
11. Jin, H.; Gao, X.; Xi, H.W. Design and shock environment analysis of medium floating shock platform. *Mod. Appl. Phys.* **2019**, *10*, 66–71. [CrossRef]
12. Zhang, W. Numerical simulation for shock resistivity of shipboard equipment on floating shock platform. *J. Vib. Shock* **2010**, *29*, 60–63.
13. Jun, G.; Yang, Y.; Zhang, Y.; Feng, L.H. The Spherical Shock Factor Theory of a FSP with an Underwater Added Structure. *Shock Vib.* **2019**, *2019*, 7080941. [CrossRef]
14. Zhang, L.; Du, Z.P.; Wu, J.B. Low-frequency shock response data analysis of underwater explosion test of 200-ton class floating shock platform. *Chin. J. Ship Res.* **2018**, *13*, 60–65.
15. Feng, L.H.; Han, L.; Yang, Y. A design of oblique baffle structure for optimizing the input environment of a large-scale floating shock platform. *Chin. J. Ship Res.* **2019**, *14*, 14–20.
16. Zhang, H.N.; Zhang, C.H.; Zhang, L. Research on shock environment characteristics of large-scale floating shock platform. *Chin. J. Ship Res.* **2023**, *10*, 2023101702. [CrossRef]
17. Keil, A.H. The Response of Ships to Underwater Explosions. *Trans. Soc. Nav. Archit. Mar. Eng.* **2010**, *69*, 43. Available online: http://hdl.handle.net/1721.3/48983 (accessed on 3 December 2023).
18. Feng, L.H.; Yao, X.L.; Wang, Y. Engineering Prediction Method of Ship Impulsive Environment Based on Empirical Eigenfunction. *Shipbuild. China* **2010**, *51*, 65–76.
19. Gu, B.; Lang, T.Q.; Liu, C.D. Research on shock environment of ship based on sample library method. *Ship Sci. Technol.* **2013**, *35*, 11–17.
20. Cunniff, P.F.; O'hara, G.J. A procedure for generating shock design values. *J. Sound Vib.* **1989**, *134*, 155–164. [CrossRef]
21. *HJB715-2016*; Ship Shock Response Spectrum. People's Liberation Army Navy: Beijing, China, 2017.
22. Han, L.; Feng, L.H.; Zhang, L. Environmental characteristics of submarine equipment's shock test section. *J. Vib. Shock* **2019**, *38*, 80–85. (In Chinese)
23. *GJB1060.1-91*; Ship Environmental Conditions Requirements-Mechanical Environment. National Defense Science and Technology Commission: Beijing, China, 1991.
24. *ISO/WD-18431-4*; Mechanical Vibration and Shock Signal Processing, Part4: Shock Response Spectrum Analysis. International Organization for Standardization: Geneva, Switzerland, 2007.
25. Hobbacher, A. *Recommendations for Fatigue Design of Welded Joints and Components*; Springer International Publishing: Cham, Switzerland, 2016.